Proceedings of Meetings on Acoustics

Volume 18, 2012 http://acousticalsociety.org/

164th Meeting of the Acoustical Society of America
Kansas City, Missouri
22 - 26 October 2012

Session 3aNS: Noise

3aNS3. Modification of directivity curves for a rocket noise model

Michael M. James*, Alexandria R. Salton, Kent L. Gee, Tracianne B. Neilsen, Sally A. McInerny and R. Jeremy Kenny

***Corresponding author's address: Blue Ridge Research and Consulting, 29 N Market St, Suite 700, Asheville, NC 28801, Michael.James@BlueRidgeResearch.com**

The spatial extent and downstream origin of rocket noise sources can significantly impact the physical interpretation of directivity index measurements. Valuable updates to historical rocket noise directivity indices, based on recent measurements of Space Shuttle reusable solid rocket motor (RSRM) boosters have been published by Haynes and Kenny (AIAA paper 2009-3160). However, measurements at a radial distance of 80 nozzle diameters from the RSRM nozzle exit plane are insufficient to be called the far field at low frequencies and thus require modification to the apparent source origin prior to their use in the empirical sound pressure level prediction methodologies, such as described in NASA SP-8072 (1971). In this analysis, estimates of plume source sound power level as a function of distance along the plume axis are combined with frequency-dependent, far field directivity indices to predict sound pressure level as a function of angle and range. With geometric modifications in place, the predicted overall sound directivity more closely matches that estimated by convective Mach number alone. These improved, more physically-based directivity indices will aid in the accurate prediction of full-scale launch vehicle noise, which is a key factor in estimating both vibroacoustic loading and environmental noise concerns.

Published by the Acoustical Society of America through the American Institute of Physics

 [DOI: 10.1121/1.4870986]
Received 20 Jan 2014; published 31 Mar 2014

INTRODUCTION

The accurate prediction of full-scale launch vehicle noise is a key factor in estimating vibroacoustic loading on vehicles, payloads, and launch structures. Despite being developed over four decades ago, the empirical models contained within NASA SP-8072[1] remain the only noise prediction methods that connect source parameters (thrust, sound speed within the plume, etc.) to radiated sound pressure levels. In this model, estimates of plume source sound power level as a function of distance along the plume axis are combined with frequency-dependent, far-field directivity indices to predict sound pressure level as a function of angle and range.

The empirical model requires that the plume be divided into conical sections, as shown schematically in Figure 1.The contribution to the sound pressure level, L_p, associated with the i^{th} plume subsource, from a given frequency, *f*, predicted at a given observer position (r, θ) may be written as

$$L_{p,i}(f, r, \theta) = L_{W,i}(f) - 10\log[4\pi R_i^2] + \mathrm{DI}(f, \theta), \tag{1}$$

where R_i is the distance from the i^{th} plume slice to the observation location at (r, θ), and $L_{W,i}(f)$ is the power associated with the corresponding subsource. The directivity indices $\mathrm{DI}(f, \theta)$ come from far-field measurements. The total sound pressure level as a function of position and frequency, $L_p(f, r, \theta)$, is found by a summation over the subsources. Updates to the source sound power allocation and the DI, based on recent measurements of Space Shuttle reusable solid rocket motor (RSRM) boosters[2,3] and computational fluid dynamics simulations, have been investigated by Haynes and Kenny.[4] These updates have been used by Plotkin and Vu[5,6] in launch pad noise prediction models.

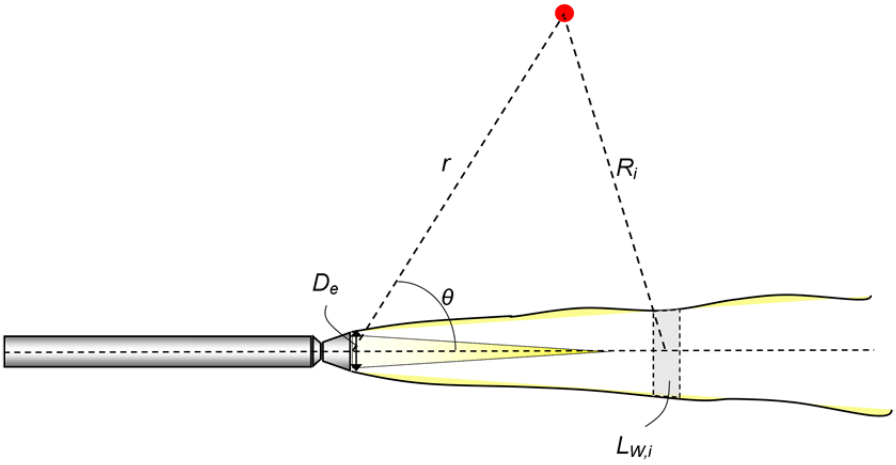

FIGURE 1. Schematic illustrating the geometry of the observer position (red dot) relative to the nozzle and the *i*th plume slice.

As with any model, it is important to examine the governing assumptions and methodologies. A companion paper[7] provides a comparison of recent near-field pressure measurements[8] of an Orion-50S XLG solid rocket motor to empirical curves in SP-8072[1] and shows $L_{W,i}$ as a function of source parameters. The current article describes the impact of geometric considerations in measuring and applying the DI to predict $L_p(f,r,\theta)$ using either of the two distributed source methods (DSM) proposed in SP-8072. We first review the assumptions made in determining $\mathrm{DI}(f,\theta)$ and show how these assumptions can be violated for an extended source whose spatial distribution is frequency-dependent. Based on an adjustment of source location as a function of frequency, modified DI for the RSRM data are developed. In conclusion, maps of $L_p(f,r,\theta)$, based on the original and modified $\mathrm{DI}(f,\theta)$, are shown and used to estimate the onset of the geometric far field.

APPARENT SOURCE LOCATIONS FOR RSRM

In order to describe how the measured $\mathrm{DI}(f,\theta)$ from the RSRM may be influenced by geometric considerations, we first need to provide an estimate of aeroacoustic source locations within the plume as a function of frequency. To keep the model simple, we employed the assumption made in the SP-8072 distributed source method (DSM-1) that uses a technique of assigning each frequency a unique source location along the flow axis, i.e., the radiated power from one frequency radiates from one position in the plume. The RSRM pressure spectra used to determine these locations was taken at multiple downstream distances along a line parallel to the centerline at an offset distance of 18 nozzle diameters (D_e). For the RSRM, the peak frequency of the maximum sound level as a function of position is displayed as circles in Figure 2, superposed on the SP-8072 curves, in terms of Strouhal number. The dashed line is a curve fit to the near-field data, which is used as the source distribution in the DSM-1 model to represent the frequency distribution as a function of apparent axial source position. For the RSRM, the engine diameter and velocity used to calculate the Strouhal number are 3.88 m and 2454 m/s, respectively.

As with the previous Orion-50S XLG analysis,[7] the estimated RSRM source location follows that of the SP-8072 undeflected plume data sets over their frequency ranges. However, unlike the Orion-50S XLG data, the high-frequency trends for RSRM match that of the plume deflected by an "open scoop." Though perhaps coincidental, Gee *et al.*[3] provided evidence that the RSRM measured levels were impacted by the plume impinging on the hillside toward which they were fired, which may perform a role similar to an "open scoop" deflector. In any event, these estimated source locations as a function of frequency can be used to produce modified $\mathrm{DI}(f,\theta)$.

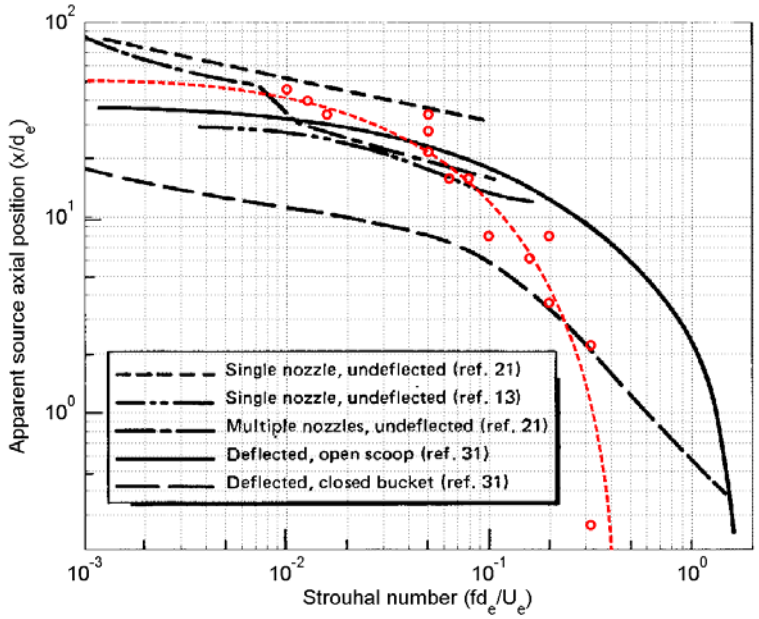

FIGURE 2. Comparison of the apparent axial source position as a function of Strouhal number for the RSRM data and the empirical curves from SP-8072. The circles correspond to the peak frequencies in pressure levels at the measurement locations and the red dashed line is the curve fit.

DIRECTIVITY INDICES: MEASUREMENT CONSIDERATIONS

In utilizing a polar arc to estimate $\mathrm{DI}(f,\theta)$ for any source, there are a number of considerations and/or assumptions.[9] The first assumption made is that $r \gg l$, where l is the characteristic length of the source. This describes the location of the geometric far field, where the source can be assumed to be compact. The second assumption is that the array is centered on the source location, such that r is the same for each angle. Figure 3 shows example microphone locations, set to match the RSRM geometry, in that they are located at $80D_e$ and centered on the nozzle. Other assumptions that come into play are that outdoor measurements are not significantly impacted by wind or terrain or that the propagation of the noise is linear. This last assumption is particularly onerous, as the noise propagation from military jets[10-14] and large rockets[15-19] is known to be nonlinear. Because the nonlinearity is frequency and level dependent, the severity of the nonlinear effects are not uniform as a function of angle for a directional source, causing an ill-defined effect on $\mathrm{DI}(f,\theta)$. Consequently, the models described in SP-8072 neglect a key feature of the propagation. However, because nonlinearity may have a lesser effect on propagation of relatively low frequencies that dominate overall sound pressure level, there is still some possible utility in applying such an empirical model.

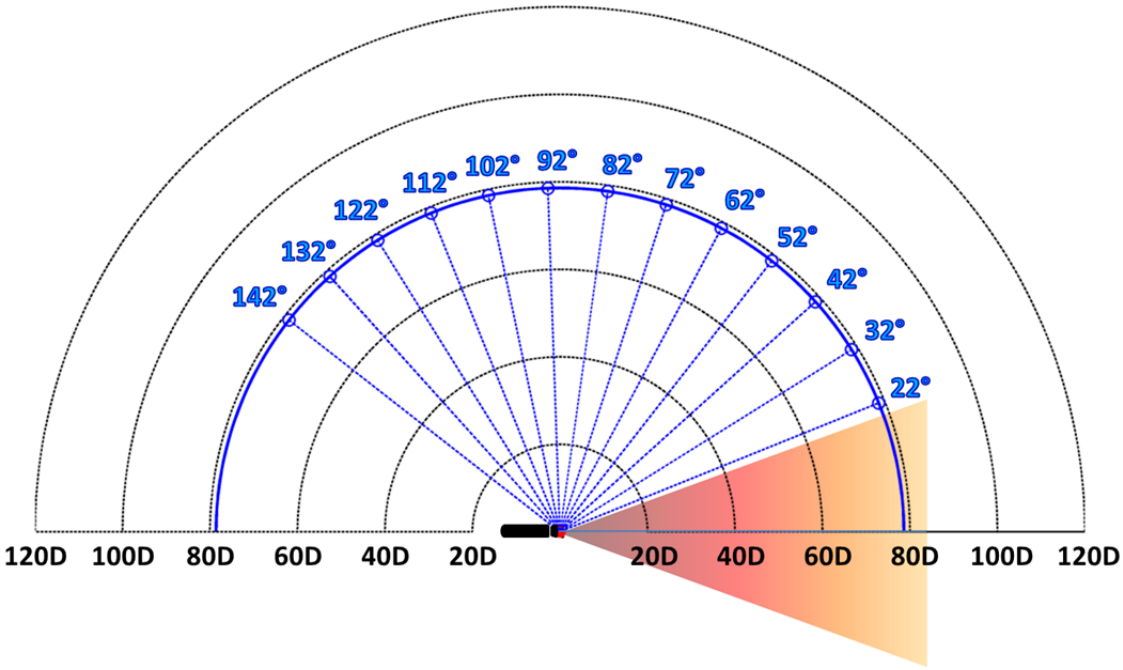

FIGURE 3. Measurements for the RSRM test located at $80D_e$ in 10° increments relative to the nozzle exit plane. The listed angles are relative the nozzle and exhaust axis, which were vectored at 4° from the center line. (See Fig. 9 of Ref. [4].)

The schematic in Figure 3 illustrates the assumption often made that the noise at all frequencies originates from the nozzle as a compact source. If instead, the apparent source axial position, as illustrated in Figure 2 is used as the origin of the contributions from a certain frequency, the angles and distances of the measurement locations shift. In this way, estimates of the dominant source location can be used to alter the $\mathrm{DI}(f,\theta)$ by adjusting the angle from the apparent source to a measurement location and using spherical spreading to correct for the nonuniform distance as a function of angle. This process can be repeated for each $\mathrm{DI}(f,\theta)$. As an example, Figure 2 predicts the dominant source region for 10 Hz ($\mathrm{St} \approx 0.016$) to be approximately $31D_e$ downstream of the nozzle. A comparison between Figure 3 and Figure 4 shows that the $80D_e$ measurement arc is far from being centered on the 10-Hz noise source region. This shift is expected to have a significant impact on $\mathrm{DI}(f,\theta)$ for low-frequency sound pressure level predictions whose source regions are farthest from the nozzle.

Before examining how a shift in angle and correction for non-uniform measurement distances affects $\mathrm{DI}(f,\theta)$, one might ask why not simply make measurements at greater distances than $80D_e$ to solve the problem of being within the geometric near field. However, the far-field region is where the other assumptions – the absence of atmospheric and environmental effects, as well as that of cumulative nonlinear propagation – are more likely to be violated, making measured $\mathrm{DI}(f,\theta)$ suspect for other reasons.

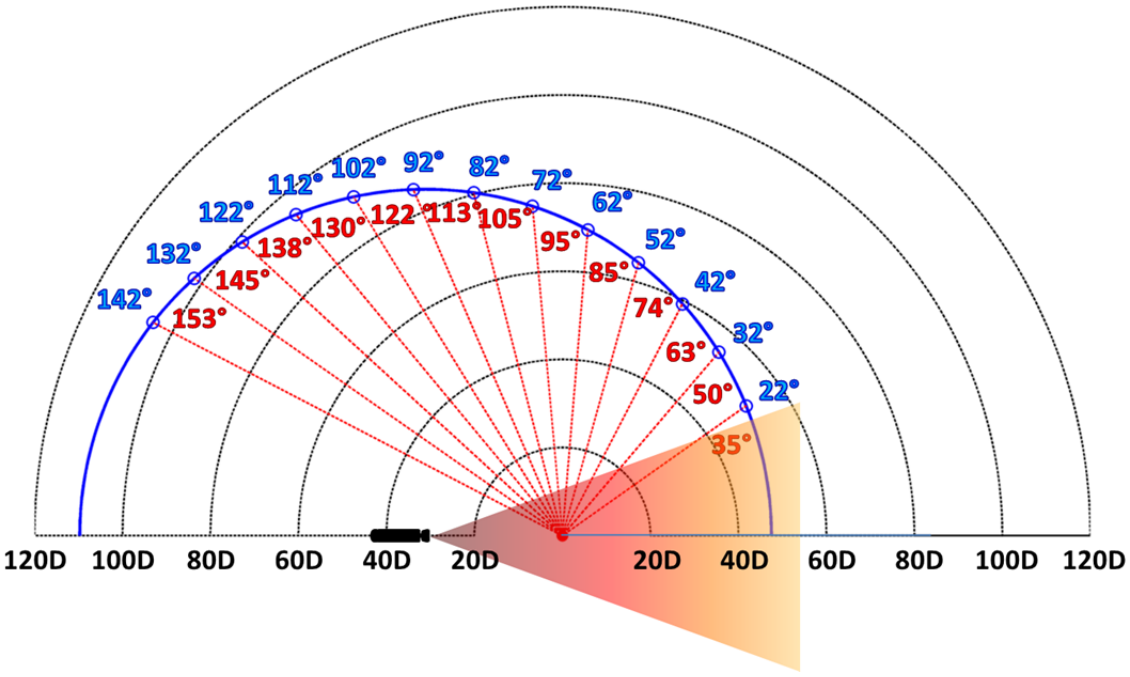

FIGURE 4. Modified angles (shown in red) relative to a shifted dominant source location at 10 Hz (St ≈ 0.016) corresponding to the RSRM measurement locations.

MODIFICATION TO DIRECTIVITY INDICES

The apparent source locations were used to adjust the DI(f,θ). The original and modified DI(f,θ), from the measurements, which were located at $80D_e$, at 11 angular positions from 22° to 142° relative to the exhaust axis, are shown as a function of one-third octave (OTO) band number and frequency in Figure 5 and Figure 6. As is expected based on source location arguments, the DI(f,θ) at low frequencies are most impacted by geometric considerations. The influence of source location on DI(f,θ) is evaluated further in Figure 7, which shows the difference between the original and modified DI(f,θ), in decibels, as a function of OTO band number and angle. Above OTO band 20 (100 Hz, St ≈ 0.16), there is very little change in the source directionality between the original and modified curves, which corresponds to the apparent source location approaching the nozzle as frequency increases (see Figure 2). However, the narrowing of DI(f,θ) at high frequencies in both Figure 5 and Figure 6 above OTO band 30 (1000 Hz, St ≈ 1.6), as noted by Haynes and Kenny,[4] contradicts the trends of published directivity curves in SP-8072. We believe a possible explanation for this feature of the data is the previously mentioned nonlinear effects, which result in nonuniform attenuation at the high frequencies with angle, tending to further emphasize the highest levels along the maximum radiation direction.[11]

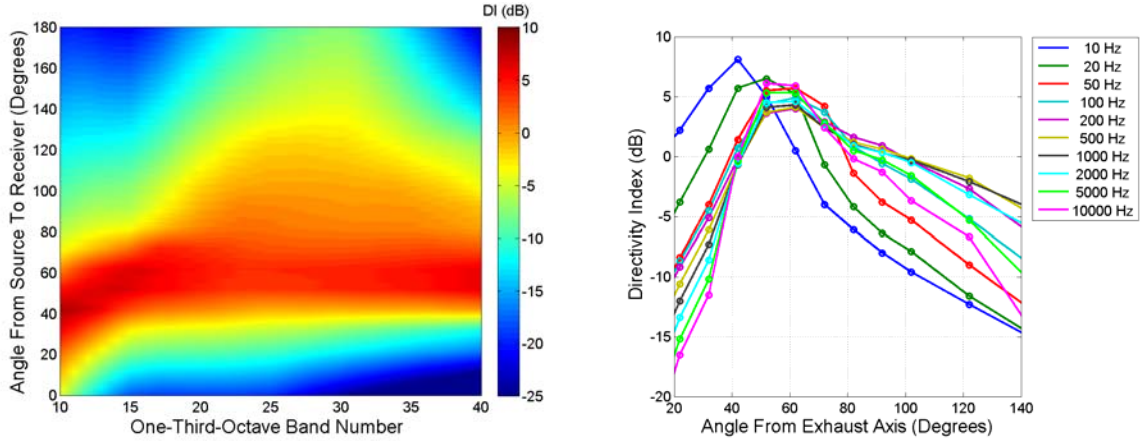

FIGURE 5. Original directivity indices as a function of frequency relative to the exhaust axis.

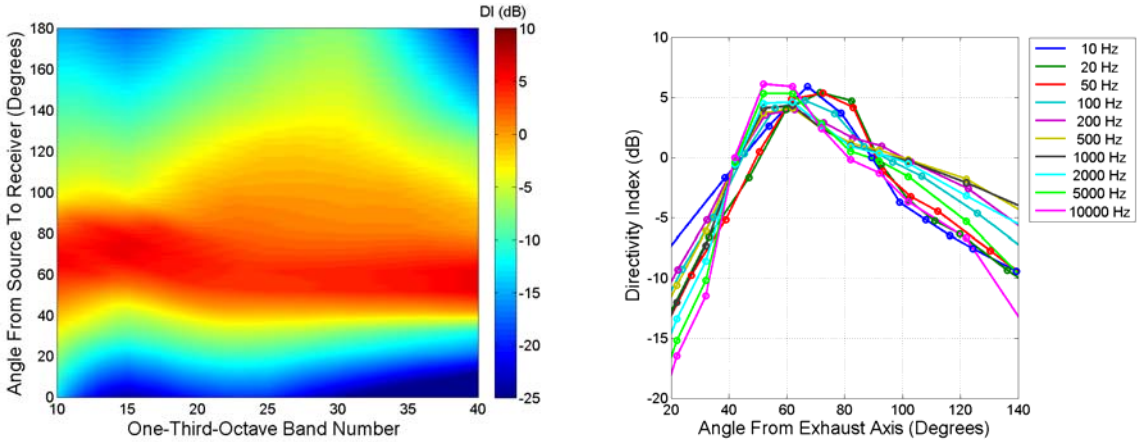

Figure 6 Modified directivity indices as a function of frequency relative to the modified apparent axial source locations.

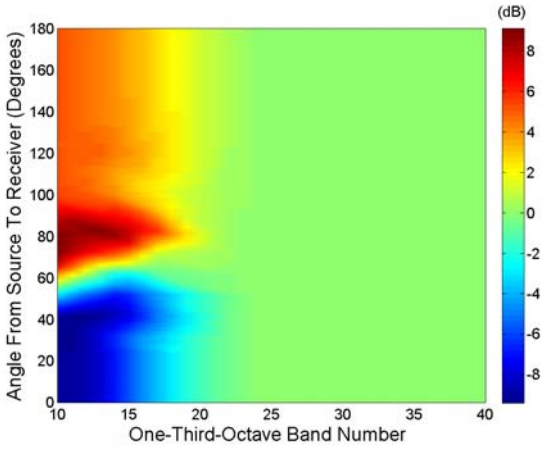

FIGURE 7. Difference, in decibels, as a function of angle and one-third octave band number between the original and modified DI (shown in Figure 5 and Figure 6, respectively).

APPLICATION OF MODIFIED DIRECTIVITY INDICES

As an initial application, the modified DI(f,θ) are used to predict the OASPL radiation from the RSRM. The originally measured and modified curves, presented in Figure 5 and Figure 6, respectively, have been used in place of the published DI(f,θ) in SP-8072's DSM-1 and DSM-2 prediction models. These two different sets of DI(f,θ), along with $L_{W,i}(f)$, from a DSM-1 model based on the apparent axial source locations shown in Figure 2, were used to obtain predicted band pressure levels and OASPL as a function of position. The four predicted OASPL maps (from methods DSM-1 and 2 for the two sets of DI(f,θ)) are displayed in Figure 8 through Figure 11. For both source models, use of the modified DI(f,θ) substantially changes the directionality of the OASPL radiation by approximately 14°, from 51° to 65°. In the far field, the two source models yield a very similar result, but in the near field, the choice of source allocation model matters significantly. Note that in allocating the overall radiated power across frequency and the plume slices with the SP-8072 in Figure 10 and Figure 11, $L_{W,i}$ (see Fig. 13 in Ref. [1]) had to be adjusted by ~2 dB in order to conserve energy. This is an issue in the original model formulation that appears to be undocumented to date and merits further investigation.

With the modified DI(f,θ), the new predicted overall directivity angle appears to more closely match that predicted by an estimation of the physical properties used in producing the source allocation model in the first place. The overall directivity angle is controlled by the convective Mach number of the plume, M_c, such that $\theta_{rad} = \cos^{-1}\left(\frac{1}{M_c}\right)$. The Oertel-Patz[20, 21] convective Mach number is defined as

$$M_c = \frac{U_e + 0.5c_e}{c_0 + c_e}, \tag{2}$$

where U_e is the plume exit velocity (≈2454 m/s), c_e is the speed of sound at the nozzle exit (≈780 m/s), and c_0 is the ambient sound speed (≈345 m/s). This results in M_c ≈2.3 and θ_{rad} ≈65°. The predicted maximum radiation direction obtained with the modified directivity indices is more reasonable, further suggesting the importance of geometric considerations in the use of this empirical model.

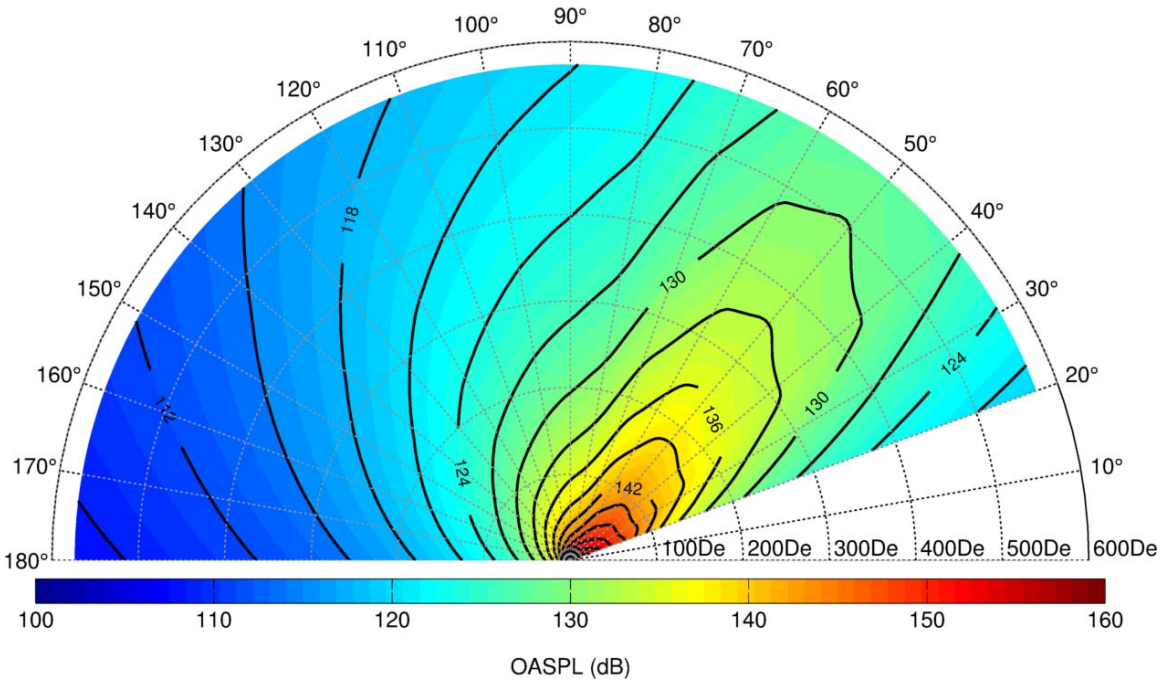

FIGURE 8. Predicted OASPL with original DI for RSRM with DSM-1.

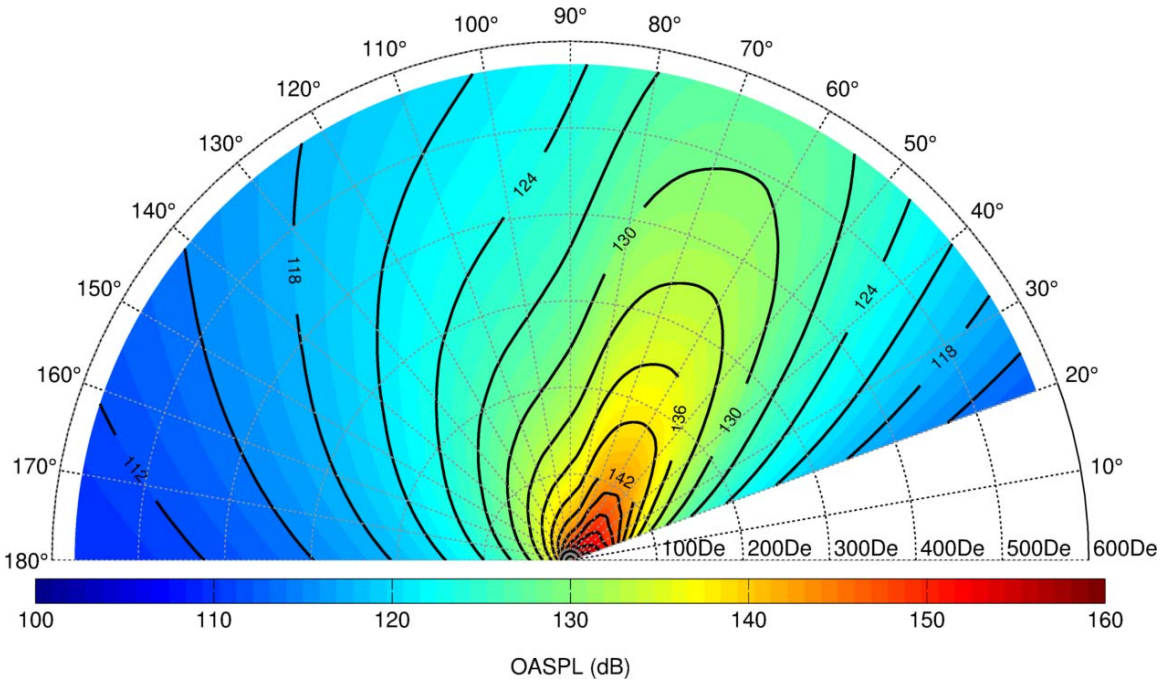

FIGURE 9. Predicted OASPL with modified DI for RSRM with DSM-1.

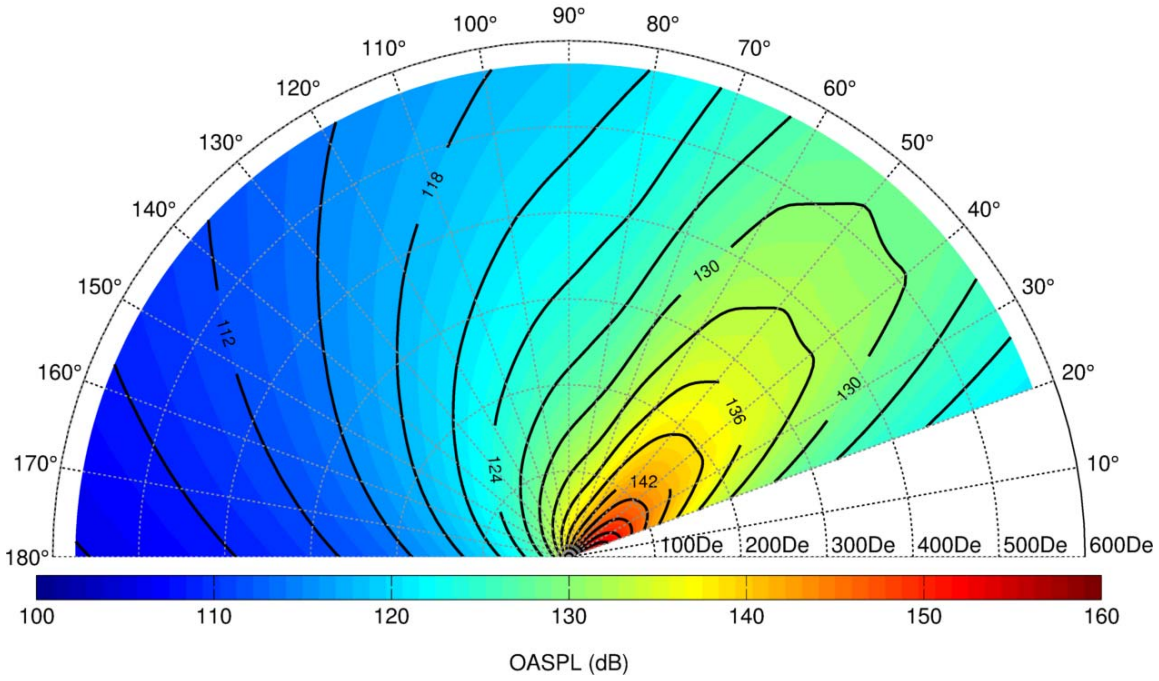

FIGURE 10. Predicted OASPL with original DI for RSRM and DSM-2

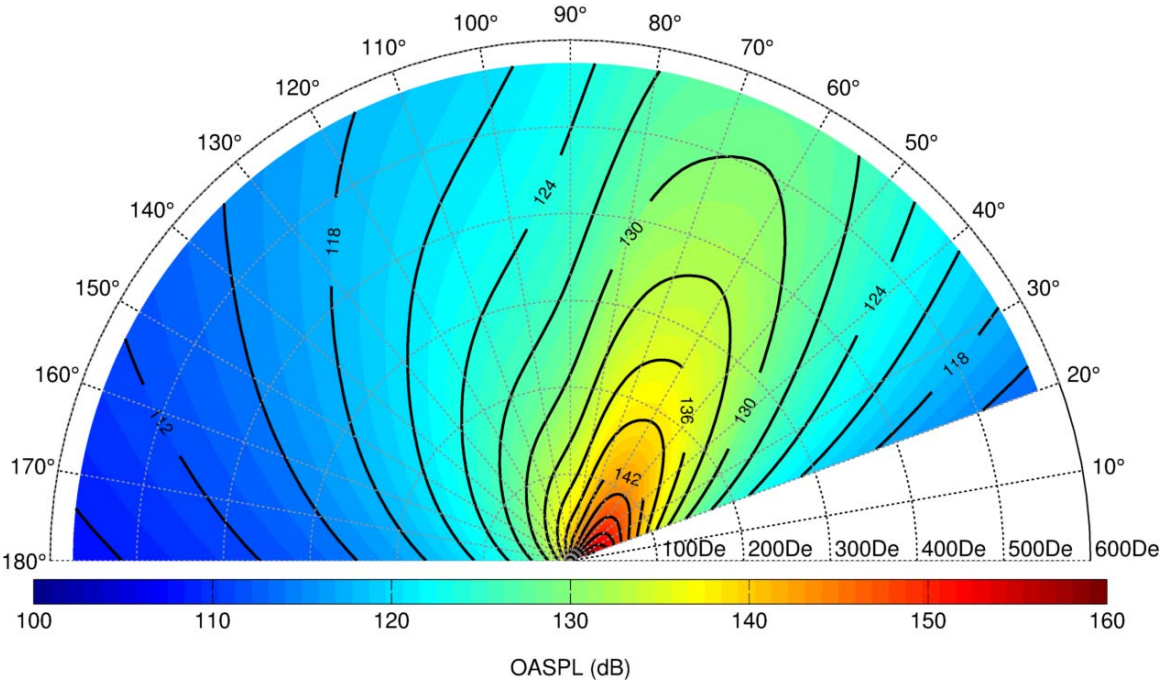

FIGURE 11. Predicted OASPL with modified DI for RSRM with DSM-2.

The spatial extent of the source and the predicted onset of the geometric far field can be investigated using the predicted OASPL maps from the modified indices in Figure 9 and Figure

11. Convergence of the peak directivity angle as calculated using the DSM-1 and DSM-2 methods effectively indicates the distance at which the source may be considered relatively compact. This analysis shown in Figure 12, predicts that the far field is approached in the 200-300 D_e range. This is remarkable – that the far field for the RSRM may not be reached until distances on the order of 1 km, but is attributable to the large-scale, distributed nature of the source.

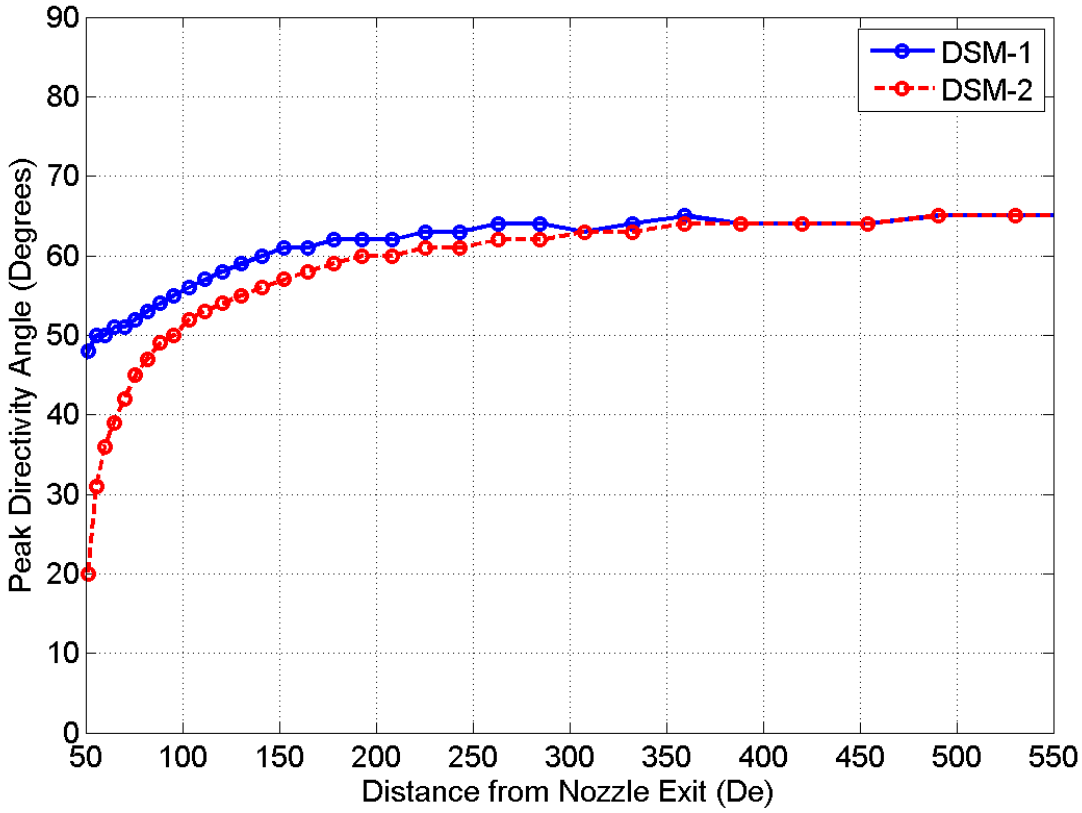

FIGURE 12. Analysis of apparent peak directivity angle in Figure 9 and Figure 11, in degrees and relative to the nozzle, as a function of distance.

CONCLUDING DISCUSSION

The analysis has shown that the spatial extent and downstream origin of rocket noise sources can significantly impact the physical interpretation of directivity index measurements. Measurements at a radial distance of 80 nozzle diameters from Space Shuttle reusable solid rocket motor (RSRM) nozzle exit plane are insufficient to be called the far field and thus require modification prior to their use in the empirical sound pressure level prediction methodologies described in NASA SP-8072. With geometric modifications in place, the predicted overall sound directivity more closely matches that estimated by convective Mach number alone.

Both this paper and the companion paper[7] have used recent near and far-field measurements of solid rocket motor noise to explore the assumptions, physical meaning, and use of decades-old

sound radiation models for rocket noise. Although the methodologies of SP-8072 appear to have some merit (given that their empirical curves were developed from databases of jet and rocket noise measurements), significant work remains to benchmark their sound pressure level predictions against modern near and far-field measurements of rocket noise. However, because full-spectrum directivity indices that meet assumptions, e.g., far-field and linear propagation assumptions, are going to be difficult to come by, opportunities to evaluate such benchmarks are likely to be limited. Consequently, near-field approaches that measure and predict the magnitude and direction of energy flux, i.e., vector intensity, merit further investigation. [8,22-25]

ACKNOWLEDGMENTS

This work has been supported by a Small Business Innovation Research (SBIR) program sponsored by NASA Stennis Space Center. The authors wish to thank Dr. William W. St. Cyr of NASA Stennis Space Center, and Alliant Techsystems Inc. for supporting the Blue Ridge Research and Consulting, LLC and Brigham Young University team.

REFERENCES

[1] K.M. Eldred, "Acoustic loads generated by the propulsion system," NASA SP-8072, (1971).
[2] R. J. Kenny, C. Hobbs, K. Plotkin, and D. Pilkey, "Measurement and characterization of Space Shuttle solid rocket motor plume acoustics," AIAA paper 2009-3161, May 2009.
[3] K. L. Gee, J. H. Giraud, J. D. Blotter, and S. D. Sommerfeldt, "Energy-based acoustical measurements of rocket noise," AIAA paper 2009-3165, May 2009.
[4] J. Haynes and R. Kenny, "Modifications to the NASA SP-8072 Distributed Source Method II for Ares I lift-off environment predictions", AIAA paper 2009-3160, May 2009.
[5] K. J. Plotkin and B. T. Vu, "Further development of a launch pad noise prediction model," J. Acoust. Soc. Am. **130**, 2510 (2011).
[6] K. J. Plotkin and B. T. Vu, "Extension of a launch pad noise prediction model to multiple engines and directional receivers," J. Acoust. Soc. Am. **132**, 1991 (2012).
[7] M. M. James, A. R. Salton, K. L. Gee, T. B. Neilsen, and S. A. McInerny, "Full-scale Rocket Motor Acoustic Tests and Comparisons with Empirical Source Models," Proc. Mtgs. Acoust. (2014).
[8] M. M. James and K. L. Gee, "Advanced acoustic measurement system for rocket noise source characterization," Proc. Internoise 2012, paper in12_1127 (2012).
[9] J. H. Giraud and K. L. Gee, "Directivity indices for rocket noise modeling: Measurement considerations," J. Acoust. Soc. Am. 127, 1772 (2010).
[10] K. L. Gee, T. B. Gabrielson, A. A. Atchley, and V. W. Sparrow, "Preliminary analysis of nonlinearity in military jet aircraft noise propagation," AIAA J. **43**, 1398-1401 (2005).
[11] K. L. Gee, V. W. Sparrow, M. M. James, J. M. Downing, C. M. Hobbs, T. B. Gabrielson, and A. A. Atchley, "The role of nonlinear effects in the propagation of noise from high-power jet aircraft," J. Acoust. Soc. Am. **123**, 4082-4093 (2008).
[12] K. L. Gee, J. M. Downing, M. M. James, R. C. McKinley, R. L. McKinley, T. B. Neilsen, A. T. Wall, "Nonlinear Evolution of Noise from a Military Jet Aircraft during Ground Run-up," AIAA paper 2012 -2258**.**
[13] K. L. Gee, T. B. Neilsen, J. M. Downing, M. M. James, R. L. McKinley, R. C. McKinley, and A. T. Wall, "Near-field shock formation in noise propagation from a high-power jet aircraft," J. Acoust. Soc. Am. **133**, EL88-EL93 (2013)**.**

[14] K. L. Gee, T. B. Neilsen, M. B. Muhlestein, A. T. Wall, J. M. Downing, and M. M. James, "On the evolution of crackle in jet noise from high-performance engines, AIAA paper 2013-2190.
[15] S. A. McInerny, "Launch vehicle acoustics Part 2: Statistics of the time domain data," J. Aircraft **33**, 518-523 (1996).
[16] S. A. McInerny and S. M. Olcmen, "High-intensity rocket noise: Nonlinear propagation, atmospheric absorption, and characterization," *J. Acoust. Soc. Am.*, **117**(2) pp. 578-591 (2005).
[17] C. L. Morfey, "Aperiodic signal propagation at finite amplitudes: some practical applications," in *Proceedings of the 10th International Symposium on Nonlinear Acoustics*, Kobe, Japan (1984).
[18] M. B. Muhlestein, K. L. Gee, T. B. Neilsen, and D. C. Thomas, "Prediction of nonlinear noise propagation from a solid rocket motor," submitted to J. Acoust. Soc. Am. (2013).
[19] M. R. Shepherd, K. L. Gee, and M. S. Wochner, "Numerical study of finite-amplitude source reconstruction in one-dimension," J. Acoust. Soc. Am. **124**, 2516 (2008).
[20] H. Oertel and G. Patz, "Wirkung von unterschallmanteln auf die Machwellen in der umgebung von Uberschallstrahlen," ISL Report RT 505/81. Institut Franco-Allemand De Recherches, Saint-Louis, France.
[21] W. J. Baars, C. E. Tinney, N. E. Murray, B. J. Jansen, and P. Panickar, "The effect of heat on turbulent mixing noise in supersonic jets," AIAA Paper 2011-1029.
[22] S. M. Jaeger and C. S. Allen, "Two-dimensional sound intensity analysis of jet noise," AIAA Paper 93-4342.
[23] T. A. Stout, K. L. Gee, T. B. Neilsen, A. T. Wall, D. W. Krueger, and M. M. James, "Preliminary Analysis of Acoustic Intensity in a Military Jet Noise Field," Proc. Mtgs. Acoust. **19**, 040074 (2013).
[24] K. L. Gee, J. H. Giraud, J. D. Blotter, and S. D. Sommerfeldt, "Near-field vector intensity measurements of a small solid rocket motor," *J. Acoust. Soc. Am.* **128**, EL69–EL74 (2010).
[25] K. L. Gee, J. H. Giraud, J. D. Blotter, and S. D. Sommerfeldt, "Energy-based acoustical measurements of rocket noise," AIAA Paper 2009-3165.